J Solid State Electrochem (2006) 10: 949–958
DOI 10.1007/s10008-005-0018-6

ORIGINAL PAPER

Antonio Doménech · Maria Teresa Doménech-Carbó

Chronoamperometric study of proton transfer/electron transfer in solid state electrochemistry of organic dyes

Received: 24 February 2005 / Revised: 9 March 2005 / Accepted: 28 April 2005 / Published online: 2 August 2005

Abstract Chronoamperometric data for proton-assisted reduction/oxidation of a series of dyes, namely, alizarin, purpurin, luteolin, morin, and indigo are compared with the predictions of the model of Lovric and Scholz for redox conductive microcrystals assuming electron and proton hopping in mutually perpendicular directions. Upon the attachment of solid dye microparticles to paraffin-impregnated graphite electrodes in contact with aqueous electrolytes in the pH range between 4 and 7, an excellent agreement between theory and experimental data was obtained. The diffusion coefficients of electrons and protons across dye microcrystals were estimated as 5×10^{-7} cm^2 s^{-1} and 1×10^{-10} cm^2 s^{-1}, respectively.

Introduction

The voltammetry of microparticles is an increasingly growing research field focused in the electrochemistry of solid nonconducting microparticles attached to inert electrodes in contact with selected electrolytes. Along the last decade, the scope of this methodology has experienced a considerable growth, including from the analysis of high-temperature superconductors to mineral, alloys, glasses and organic compounds [1–4].

Application of the voltammetry of microparticles, to the identification and characterisation of organic compounds has claimed attention in recent years. From the seminal work of Scholz et al. [5], the voltammetry of different organic compounds [6–8] and organic-based materials [9–11] has been described in the last years.

In this context, Lovric and Scholz [12, 13] and Oldham [14] formulated theoretical models for explaining electron transfer processes involving nonconducting solids. In the more recent version reported by Schröder et al. [15] electron transfer processes in a solid compound characterised by mixed ionic/electronic conductivity, involve an initial reaction at the three-phase electrolyte/particle/electrode junction further extended via transport of electrons and charge-balancing cations in perpendicular directions.

Electron transport occurs via electron hopping between immobile redox centres, whereas, ion transport must be accomplished via cation insertion and diffusion in solids such as hexacyanoferrates [3] and microporous materials such as zeolites, layered hydroxides and aluminosilicates [16]. In this context, Bond et al. have described the solid state electrochemistry of solid $[Co(mtas)_2](X)_n$ (mtas = *bis*(2-(dimethylarsino) phenyl) methylarsine; $X = BF_4^-$, ClO_4^-, BPh_4^-; $n = 2,3$) and $[M(bipy)_2\ M'(bipy)_2\ (-L)]$ (M,M′ = Ru, Os; bipy = 2.2′-bipyridyl; L = 1,4-dihydroxy-2,5-*bis*(pyrazol-1-yl)benzene) where anion insertion takes place [17–19].

In the case of much organic solids, in which in general ion insertion cannot occur, proton transfer processes appears to be the unique way for yielding solid state voltammetric processes. This requires proton transfer between the electrolyte solution and the external layer of molecules in solid microcrystals, and eventually, charge propagation across the solid via proton hopping between adjacent molecules. This situation parallels to that described by Andrieux et Savéant [20] and Wu et al. [21] for redox polymers. In the case of organic solids, however, one can expect that the propagation of electron hopping has to be significantly hindered, so that the extent of the electroactive region in which effective proton hopping occurs is limited to a shallow boundary region of the particles. The influence of the concentration of electrolyte cations was also studied by Lovric et al. [22].

A. Doménech (✉)
Departament de Química Analítica, Universitat de València,
Dr. Moliner 50, 46100, Burjassot (Valencia), Spain
E-mail: antonio.domenech@uv.es
Tel.: +34-96-3544533
Fax: +34-96-3544436

Maria Teresa Doménech-Carbó
Departament de Conservació i Restauració de Bens Culturals,
Universitat Politècnica de València, Camí de Vera, s/n, 46022,
Valencia, Spain

The current work describes a voltammetric and chronoamperometric study devoted to (1) test the applicability of such model to organic solids, and (2) to compare alternative formulations depending on the extent of possible proton hopping and electron hopping processes throughout the solid. Theory will be compared with experimental data for different indigoid, anthraquinonic and flavonoid dyes, namely, indigo (3H-indol-3-one, 2-(1,3-dihydro-3-oxo-2H-indol-2-ylidene)-1,2-dihydro), alizarin (1-hydroxy-, 2-hydroxy-, 1,2-dihydroxy-anthraquinone), purpurin (1,4-dihydroxy-, 1,8-dihydroxy-, 1,2,4-trihydroxy-anthraquinone), luteolin (3′,4′,5,7-tetrahydroxyflavone), and morin (2′,3,4′,5,7-pentahydroxyflavone). Structural formulas of such compounds are depicted in Sch. 1.

These were selected as test compounds because of: (1) their insolubility in aqueous electrolytes, and, (2) their similar solid-state electrochemistry, displaying, in all cases, reversible two electron, two-proton reduction and/or oxidation processes. Thus, solid indigo is reversibly reduced to leucoindigo and a reversibly oxidised to dehydroindigo [7, 8, 10] (see Scheme 2). Such systems enable for an eventual distinction between proton/electron gain and proton/electron loss processes. Voltammetry of indigo adsorbed on pretreated carbon paste [23] and mercury [24] electrodes and direct electrochemical reduction of indigo [25, 26] have claimed attention recently for sensing and recycling of dyes.

In agreement with literature concerning anthraquinonic and flavonoid compounds in solution, quinone groups of anthraquinonic dyes are reversibly reduced to *p*-diphenol, whereas, *o*-phenol subunits (common to flavonoids and the anthraquinonic dyes studied here) are oxidized reversibly to the corresponding quinones [27–33]. This scheme is consistent with the observed voltammetry of microparticles of anthraquinonic [9, 10] and flavonoid [10, 11] dyes.

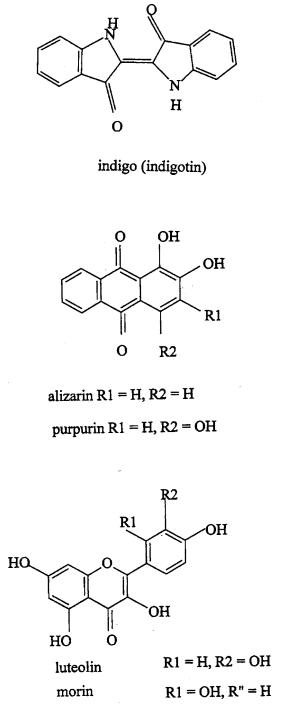

Scheme 1 Structural formulas of the compounds studied here

Experimental

Chronoamperograms, cyclic voltammograms and square wave voltammograms (CAs, CVs, and SQWVs, respectively) were performed with a BAS CV50W equipment. A standard three-electrode arrangement was used with a platinum auxiliary electrode and a AgCl (3 M NaCl)/Ag reference electrode in a cell thermostated at 298 K. Aqueous acetic/acetate (total concentration 0.50 M) and phosphate (total concentration 0.50 M) buffers (Merck) were used as supporting electrolytes.

Indigo, alizarin, purpurin, luteolin, and morin were supplied by Aldrich and used without further purification.

Paraffin-impregnated graphite electrodes (PIGEs) consist on cylindrical rods of 5-mm diameter of graphite impregnated under vacuum by paraffin. Preparation details are described in references [1–4]. To prepare sample-modified PIGEs, ca 50 mg of indigo was powdered in an agate mortar and pestle, and placed on a glazed porcelain tile forming a spot of finely distributed material and then abrasively transferred to the surface of a PIGE by rubbing the electrode over that spot of sample. Deposits containing 0.15 ± 0.02 mg of indigo were routinely used. Sample-modified PIGEs working electrodes were dipped into the electrochemical cell so that only the lower end of the electrode was in contact

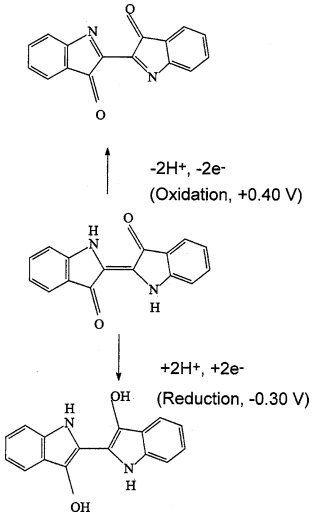

Scheme 2 Scheme of redox processes involving indigo microparticles

with the electrolyte solution. This procedure provides an almost constant electrode area and reproducible background currents.

Morphological examination of dye-modified electrodes was obtained using a Jeol JSM 6300 scanning electron microscope (SEM). The analytical conditions were: accelerating voltage 20 kV, beam current 2×10^{-9} A. Images were obtained using backscattered detector.

Theory

Let us consider a three-phase system formed by the electrolyte solution in contact with a solid particle deposited over an infinite conducting electrode. The Lovric and Scholz model [12, 13] for ion insertion processes assumes that the reaction starts at the three-phase boundary between electrode, solid particle and electrolyte. From this point, the reaction zone grows while electrons and charge-balancing cations diffuse perpendicularly along the crystal.

This model can directly extended to organic microparticles assuming that the redox reaction involves the transfer of electrons through the electrode/particle interface and the transfer of protons across the electrolyte/particle interface. The overall electrochemical process can be represented as:

$$\mathrm{A\,(solid)} + n\mathrm{H^+(sol)} + ne^- \rightarrow \mathrm{H}_n\mathrm{A(solid)} \qquad (1)$$

Here, A represents the oxidized form of the localised redox centre and H_nA its reduced (and protonated) form.

If the electron transfer/cation insertion reaction described by Eq. 1 is thermodynamically governed, it describes an equilibrium that must satisfy the Nernst equation:

$$[\mathrm{A}] = [\mathrm{H}_n\mathrm{A}]\exp\left[\frac{nF(E - E_f)}{RT}\right] = [\mathrm{H}_n\mathrm{A}]\,e^g \qquad (2)$$

where E_f is a formal potential defined as:

$$E_f = E^o + \frac{RT}{nF}\ln K + \frac{RT}{F}\ln[\mathrm{H^+}] \qquad (3)$$

In this equation, E^o is the standard potential of the redox couple A/H_nA and K represents the equilibrium constant for the reaction of proton insertion described by Eq. 1.

The propagation of the redox reaction requires simultaneous electron hopping and proton hopping between immobile redox centres. This reaction can be represented as:

$$\mathrm{H}_n\mathrm{A(solid, site1)} + \mathrm{A(solid, site2)} \rightarrow \mathrm{A(solid, site1)} + \mathrm{H}_n\mathrm{A(solid, site2)} \qquad (4)$$

Here, site 1, site 2, represent different adjacent sites alternatively occupied by the oxidized and reduced forms of the dye.

Depending on the extent of the redox reaction through the solid microparticle, different theoretical formulations can be made, namely: (a) without restricted diffusion of electrons and protons through the solid; (b) restricted proton diffusion; (c) restricted electron diffusion, (d) hindered proton diffusion, and (e) hindered electron diffusion.

The most general approach developed by Schröder et al. [15] using finite difference simulation methods, yields short-time chronoamperometric current (i)–time (t) curves (CAs). For CAs at potentials sufficiently positive/negative to make negligible the effects of electron interfacial transfer, current/time curves can be described by:

$$i = \frac{nF}{v_\mathrm{m}}\left[p\left(\frac{\Delta x_\mathrm{o}D_e^{1/2} + \Delta z_\mathrm{o}D_\mathrm{H}^{1/2}}{2\pi^{1/2}t^{1/2}}\right) + p\left(D_eD_\mathrm{H}\right)^{1/2} - 4D_\mathrm{H}\left(2D_et\right)^{1/2}\right] \qquad (5)$$

Here, D_H, D_e represent the diffusion coefficients of protons (in the x and y directions) and electrons (in the z direction), respectively, and v_m represents the molar volume ($cm^3\ mol^{-1}$) of the solid. p represents the perimeter of the three-phase electrode/electrolyte/microcrystals junction of the cuboid. Δx_o, Δz_o are the size of the three-phase junction boxes in which the crystal is divided for applying simulation procedures. It is that the electrochemical process is thermodynamically governed, isotropy for the diffusion of ions ($D_H = D_x = D_y$) and that the time experiment is sufficiently short to ensure that the diffusion-migration layer thickness is small when compared to the solid thickness.

Equation 5 corresponds to a Cottrell-like current/time dependence ($i \propto t^{-1/2}$) incorporating additional time-independent and $t^{1/2}$ terms. This last is independent of the perimeter of the three-phase junction and is attributable to a "edge effect", whereas, the time-independent term can be associated to the finite size of the crystals [15].

Equation 5 represents the theoretical CA curve corresponding to short times for unrestricted diffusion of electrons and protons (case a). The corresponding equations for cases b (restricted proton diffusion) and c (restricted electron diffusion) can be obtained by taking $D_H << D_e$, and $D_H >> D_e$, respectively. The above formulation can also be extended to the case of hindered proton diffusion, $D_H = 0$ (case d), and hindered electron diffusion, $D_e = 0$ (case e). As pointed out by Lovric and Scholz [14], there is redox conductivity even in the last two cases. Thus, if protonation reaction is limited to the surface layer; i.e., the solid particle cannot be penetrated by protons, $D_x = 0$ and the reaction is confined to the particle/

electrode interface (case d). If electron transfer across the solid is hindered ($D_z = 0$), the reaction is limited to the particle/electrolyte interface (case e).

At long times, available algebraic solutions of the diffusion problem corresponds to cases b and c. If electron diffusion is faster than proton diffusion, this last becomes rate-determining. Then, for a cuboid crystal one obtains [15]:

$$i = \frac{3.3nFHD_{\mathrm{H}}}{v_{\mathrm{m}}} \sum_{j=1}^{\infty} \exp\left[\frac{2\pi^2 D_{\mathrm{H}} t}{L^2}\right] \tag{6}$$

where L represents the breadth of the cuboid and H its height.

If proton diffusion is much faster than electron diffusion, the chronoamperometric current at long times approaches [15]:

$$i = \frac{2nFAD_{\mathrm{e}}}{Hv_{\mathrm{m}}} \sum_{j=1}^{\infty} \exp\left[\frac{\pi^2 D_{\mathrm{e}} t}{4H^2}\right] \tag{7}$$

A being the area of the crystal/electrode interface. Equations 6 and 7 are formally equivalent to CAs for thin-layer cells.

For testing alternative formulations, it is convenient to rewrite Eq. 5 in the form:

$$it^{1/2} = Bt^{-1/2} + CB - Dt \tag{8}$$

This current–time relationship applies for short-time CAs in cases a–c, while for cases d and e this relationship reduces to $it^{1/2} = Bt^{-1/2}$. That is, an "ordinary" Cottrell-type behaviour is predicted.

At long times, the CA current for cases b and c satisfies equations of the type:

$$\ln i = F - Gt \tag{9}$$

That is, a logarithmic behaviour is predicted.

The above equations can be adapted for describing the case of a deposit of N cuboid microparticles of size a.

Then Eq. 5 can be rewritten as:

$$i = nFNc\left[4a\left(\frac{f(D_e^{1/2} + D_{\mathrm{H}}^{1/2})}{2\pi^{1/2}t^{1/2}}\right) + 4a\left(D_e D_{\mathrm{H}}\right)^{1/2} - 4D_{\mathrm{H}}\left(2D_e t\right)^{1/2}\right] \tag{10}$$

where n is the number of electrons involved in the redox reaction, c ($= 1/v_{\mathrm{m}}$) represents the concentration (mol cm^{-3}) of the electroactive centres in the solid, and f represents an effective length, that corresponds to a mean size of the three-phase junction boxes in which the crystal is divided for applying simulation procedures.

Equation 6, corresponding to the case b (restricted proton diffusion), can be adapted to this N-particle formulation assuming that proton diffusion through the solid is limited to a narrow region or "active" layer of thickness δ close to the particle/electrolyte interface. Then, the "electroactive" volume will be $4a^2\,\delta$ per cuboid and Eq. 6 reduces to:

$$i = 3.3nFNacD_{\mathrm{H}} \sum_{j=1}^{\infty} \exp\left[\frac{2\pi^2 D_{\mathrm{H}} t}{4\delta^2}\right] = i_o \mathrm{e}^{-\beta t} \tag{11}$$

Similarly, for the case of restricted electron diffusion (case c), one can assume that the diffusion of electrons is constrained to a narrow layer of thickness χ adjacent to the particle/electrode interface. Then, Eq. 7 can be rewritten as

$$i = \frac{2nFNa^2 cD_e}{\chi} \sum_{j=1}^{\infty} \exp\left[\frac{\pi^2 D_e t}{4\chi^2}\right] = i_o \mathrm{e}^{-\beta t} \tag{12}$$

In Eqs. 11 and 12, i_o represents a zero-time current for the region of exponential decay of CA curves. This magnitude can be calculated as the ordinate at the origin in ln i versus t plots. The major drawback for testing such equations is the large uncertainty in estimating the number of cuboids due to: (1) it is uneasy to control the exact amount of material mechanically transferred to the electrode surface; (2) even transferring weighted amounts of the solid, the variable aggregation of the particles makes uncertain the amount of particles displaying an effective contact with the electrode.

Attempting to avoid these problems, one can relate CA data with the total charge passed during the experiments, q. This magnitude can be obtained upon integration of CA curves and is directly related with the amount of electroactive particles. Charge measurement provide a mean for directly testing the model b (restricted proton diffusion) assuming that: (1) charge transfer is completed when the reduced form, $\mathrm{H}_n\mathrm{A}$, is distributed in a tight layer of thickness δ in the lateral faces of the cuboids, and, (2) one of the faces of the cuboids are in contact with the electrode surface. Then, the total charge passed at the end of the CA experiments can be approached by:

$$q = nFN4a^2 \int_{x=0}^{x=\delta} c(x)\mathrm{d}x \tag{13}$$

$c(x)$ representing the concentration of $\mathrm{H}_n\mathrm{A}$ at a distance x from the electrolyte/particle interface when the charge transfer process is exhausted. This concentration profile is representative of the diffusion of protons through the solid. Assuming that the concentration profile at the end of the charge transfer process remains essentially identical for all cuboids, one can combine Eqs. 10 and 13, to yield a N-independent equation:

$$q = \frac{1.2ai_o}{D_{\mathrm{H}}} \int_{x=0}^{x=\delta} c(x)\mathrm{d}x \tag{14}$$

This equation predicts a linear dependence of q on i_o, a relationship that can be tested experimentally by measuring i_o and q for deposits containing different number of cuboids.

A similar treatment can in principle be proposed for the case c, restricted electron diffusion. Then, a relationship between the total charge passed and i_o similar to Eq. 14,

$$q = \frac{2\chi i_o}{D_e} \int_{z=0}^{z=\chi} c(z)\mathrm{d}z \qquad (15)$$

can be proposed.

Results and discussion

Voltammetric and chronoamperometric responses

Examination of dye-modified electrodes by scanning electron microscopy revealed that, in all the studied cases, the organic compound was deposited in aggregates of microcrystallites, whose size varied from 1 μm to 10 μm. A typical SEM image is shown in Fig. 1 for indigo.

The square wave voltammetry of indigo attached to graphite electrodes in contact with acetic/acetate buffer is shown in Fig. 2. In agreement with voltammetric data of Komorsky-Lovric et al. [7], Bond et al. [8], and Grygar et al. [10]. Indigo microparticles exhibit two reversible couples at equilibrium potentials of +0.43 and −0.30 V versus AgCl/Ag. Both couples behave reversibly, as judged by the appearance of well-defined anodic and cathodic peaks upon separate examination for the currents measured in the anodic and cathodic portions of square wave pulses [7].

Peak potentials for both couples were found to be pH-dependent, with linear variations of E_p with the pH in the pH range from 4.5 to 7.5. The slopes of such straight lines for peaks at +0.43 and −0.30 V were of 58 and 57 mV/decade, close to that expected for a two-electron/two proton reversible transfer. Accordingly, the recorded couples correspond, respectively, to the oxidation of indigo to dehydroindigo and the reduction of the parent indigo to leucoindigo, illustrated in Scheme 2.

As shown in Fig. 3a, SQWVs of anthraquinonic dyes show two well-defined peaks at −0.53 and +0.53 V (alizarin) and −0.56 and +0.50 V (purpurin) in acetic/acetate buffer (pH 4.70). Since SQWV provides simultaneous examination of both reduction and oxidation processes, the recorded peaks can unambiguously be attributed to the reduction of the quinone group and the oxidation of the *o*-phenol group of the parent compound. Both peaks behave reversibly and yield linear dependences of the peak potential on the pH in agreement with a two-electron, two-proton reversible behaviour [9, 10]. For flavonoid dyes (see Fig. 3b), only a pH-dependent reversible oxidation peak at +0.36 V (luteolin) and +0.30 V (morin), was recorded. In these cases, a reversible two-proton, two-electron oxidation of the *o*-diphenol group is operative [10, 11].

In view of the nature of the redox processes, one can expect that not only differences in electron hopping, but also in electron hopping might be recorded between the different compounds. Additionally, since the oxidation of indigo the dehydroindigo involves the loss of N–H bonds, whereas, the reduction of indigo to leucoindigo involves the formation of O–H bonds, differences between oxidation and reduction may appear.

Chronoamperometric curves can be used for testing the alternative models. In all cases, CAs were performed by application of a constant potential of a value 150 mV past the square wave voltammetric peak. This ensures that the electrochemical process is under diffusive control. In these conditions, Eqs. 5, 6, 7, 8, 9, 10, 11, 12, 13,

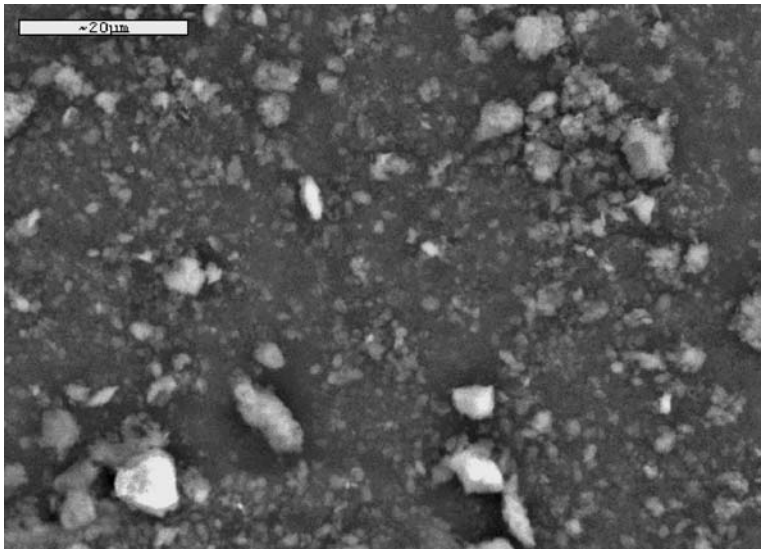

Fig. 1 SEM image of a typical deposit of indigo on graphite surfaces

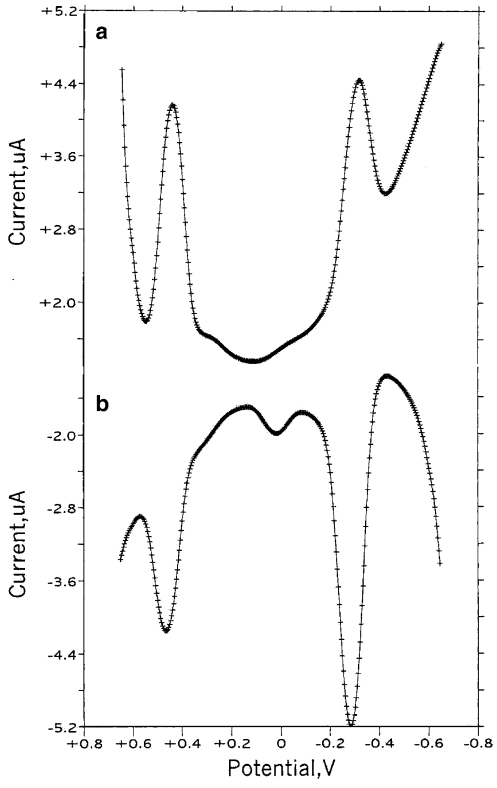

Fig. 2 SQWVs of indigo-modified PIGEs immersed into 0.50 M acetate buffer + 0.50 M phosphate buffer aqueous solution at pH 5.57. **a** Potential scan initiated at +0.65 V in the negative direction; **b** potential scan initiated at −0.65 V in the positive direction. Potential step increment 4 mV; square wave amplitude 25 mV; frequency 5 Hz

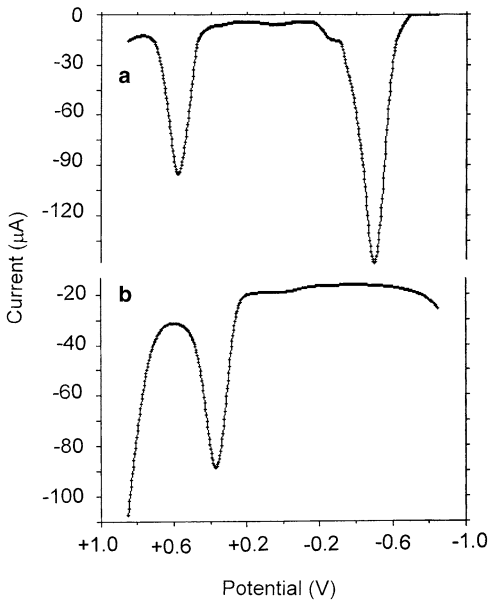

Fig. 3 SQWVs of PIGEs modified by: **a** alizarin, and **b** morin, immersed into 0.50 M acetate buffer at pH 4.70. Potential scan initiated at −0.85 V in the positive direction. Potential step increment 4 mV; square wave amplitude 25 mV; frequency 15 Hz

14 could be tested with CA data. Attempting to avoid problems associated with relatively large background currents, blank experiments were performed at bare PIGEs immersed in each one of the electrolytes. Working CA curves were obtained by subtracting the CA recorded at a bare PIGE from the CA obtained at a dye-modified electrode. Typical curves are shown in Fig. 4, corresponding to: (a) the oxidation of indigo in acetic/acetate buffer at pH 5.04, (b) the blank CA, (c) the subtracted curve. The integrated curve, yielding a direct estimate of the total charge passed is shown in Fig. 4d.

Following Schröeder et al. [15], $it^{1/2}$ versus $t^{1/2}$ plots have been used for comparing experimental data with predictions from Eqs. 5 or 10. The corresponding representation for the oxidation of indigo in phosphate buffer at pH 6.85 is shown in Fig. 5. In this representation, the product $it^{1/2}$ increases initially while time increases until a maximum value is reached at a certain transition time, t^*. From which the product $it^{1/2}$ decreases monotonically.

First of all, it should be noted that the presence of this initial rising region in the $it^{1/2}$ versus $t^{1/2}$ plot denotes that cases d and e do not apply; i.e., that neither proton diffusion nor electron diffusion are entirely hindered.

The current decay recorded at times longer than t^* defines two overlapped regions in which $it^{1/2}$ approaches successively: (1) a linear dependence on t, in agreement with Eqs. 5 and 10, and, (2) an exponential decay able to be described by Eqs. 6 or 7 (or Eqs. 11 and 12, respectively). Figure 6 shows $it^{1/2}$ versus t plots for times between 4 ms and 10 ms for the CA oxidation of indigo attached to PIGE at +500 mV in phosphate buffer (pH 6.85). Here, a linear dependence of $it^{1/2}$ versus t is obtained, in agreement with Eqs. 5 and 10. Similar results were obtained for all tested oxidation and reduction processes.

Since Eqs. 6, 7 (or 11, 12) are operative when the redox reaction is almost exhausted [15], the appearance of such exponential decay suggests that the reaction is completed in short time. First, this is in close agreement with the general theoretical framework provided by the model of Lovric and Scholz [15]: the fast current decay is demanded by combination of finite crystal size and finite diffusion space occurring in the electrochemistry of microparticles. Second, the relatively rapid current decay indicates that the redox reaction is confined to a small zone in the crystals.

Plots of ln i versus t at times ranging between 8 ms and 25 ms for the CA oxidation of different indigo deposits at pH 5.04 are shown in Fig. 7. Linear dependences between ln i and t were obtained, confirming the expectance from Eqs. 6 (or (11) or, alternatively, (7) (or (12)). The y-intercept, depending on the number of cuboids, N, varied from one deposit to another, while the slope remains almost constant. Again, similar results were obtained for all tested electrochemical processes in the studied dyes.

Extent of the redox reaction

The area under voltammetric peaks provides a direct estimate of the total amount of charge passed during the application of the potential step. For deposits containing weighted amounts of indigo between 0.10 mg and 0.60 mg, the total amount of charge falls in the range between 2 μC and 15 μC. As expected, these values are considerably lower than the total amount of indigo (3.8×10^{-7}–2.3×10^{-6} mol) whose hypothetical exhaustive two-electron oxidation or reduction should consume charges between 0.073 C and 0.444 C. Similar results were obtained for all other dyes.

Charge data suggest that the electrochemical reaction is confined to a tight zone, as expected by effect of the restricted process of proton hopping or restricted electron hopping (cases b and c, respectively) required for the propagation of charge through the organic solid.

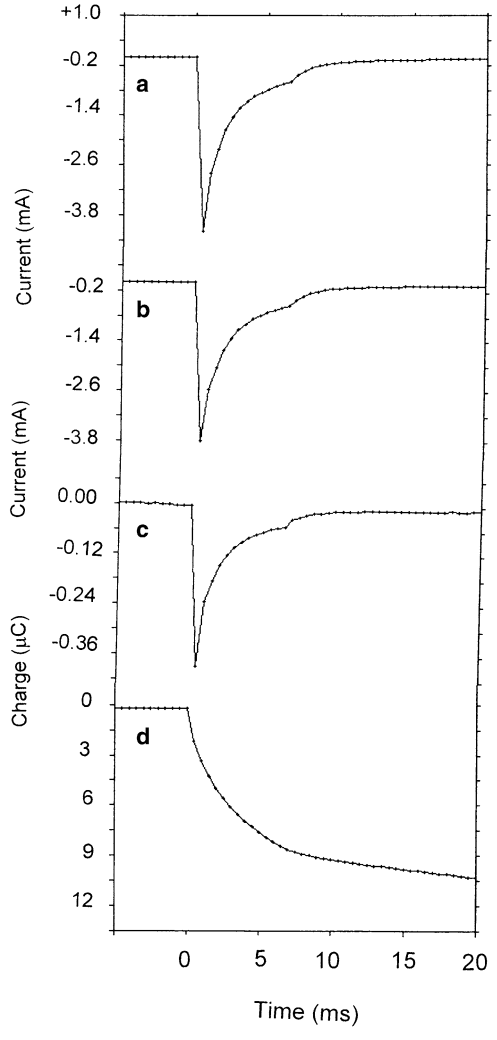

Fig. 4 CA at an indigo-modified PIGE. Applied potential: +550 mV. Electrolyte: aqueous acetate buffer (total concentration 0.50 M) at pH 5.04. **a** CA curve at indigo-modified PIGE; **b** CA curve at unmodified PIGE; **c** curve resulting from the subtraction **a**−**b**; **d** integrated curve representing charge versus time plot

Representation of the total charge passed, q, determined as the time integral of the current in CAs, as a function of i_o, determined as the ordinate at the origin of such ln i versus t plots, yields graphs such as depicted in Fig. 8 corresponding to indigo oxidation at pH 5.57. In agreement with the predictions from Eqs. 14 and 15, a linear q versus i_o dependence appears. Similar q versus i_o plots were obtained for all other dyes.

Assuming that the model b applies, the minimum thickness of the reaction layer, δ_{min}, can easily be estimated on assuming that (1) the indigo deposit is formed by cuboid microcrystals of size a (mean value ca 5×10^{-4} cm as derived from SEM/EDX data), and, (2) that all the cuboids are in contact with the electrode surface. This second assumption, however, is not realistic; as shown in Fig. 1, the indigo deposits consist of microcyrstal aggregates so that only a fraction of crystals is in contact with the electrode surface. Accordingly, charge transfer data only provides an estimate of the minimum thickness, δ_{min}, of the electroactive region of crystals.

For estimating δ_{min}, the number of cuboids, N, was calculated from the mass of the deposit, m, the density of indigo, and the cuboid size as $N=m/\rho a^3$, ρ being the density of the solid. Assuming that the reaction layer occupies the lateral faces of the cuboids, the volume of that reaction layer, V^*, can be approached by the expression $V^*=4\delta_{min}a^2N$. Assuming that the deposit of indigo is composed by a set of cuboid microcrystals of 5 μm size, for deposits of 1.5 mg, and taken a density of 1.35 g cm^{-3}, the number of cuboids is of 8.89×10^5 and then, the total length of the three-phase junction is of 1,780 cm.

The values calculated for several a values are shown in Table 1. Although a detailed account of the shape and size distribution of the indigo particles is required for properly estimate the thickness of the reaction layer, the obtained values of δ_{min} do not vary significantly for cuboids size between 1×10^{-4} cm and 1×10^{-3} cm (δ_{min}

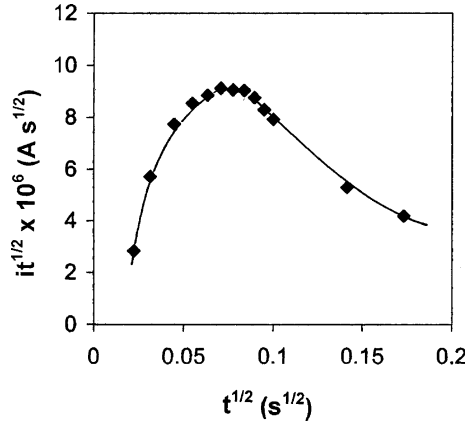

Fig. 5 Plots of the $it^{1/2}$ product versus $t^{1/2}$ for the CA oxidation of indigo at +500 mV in phosphate buffer (pH 6.85). Data from the working curve obtained by subtracting the blank curve recorded at an unmodified PIGE from that recorded at an indigo-modified PIGE

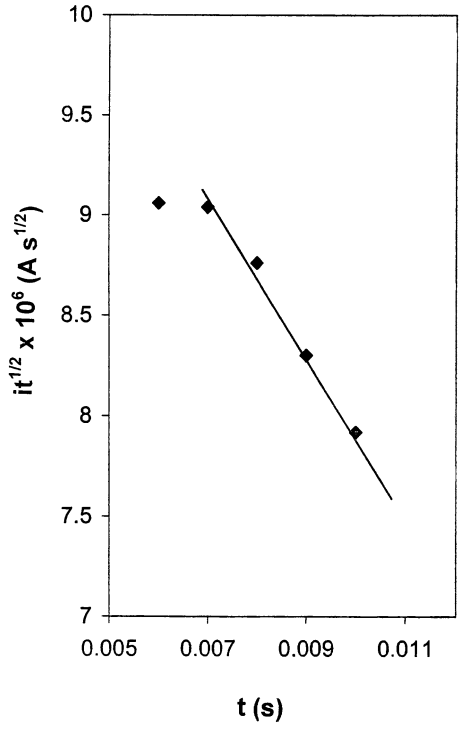

Fig. 6 Plots of $it^{1/2}$ versus t (times between 4 ms and 10 ms), for the CA oxidation of indigo attached to PIGE at +500 mV in phosphate buffer (pH 6.85). Data from the working curve obtained by subtracting the blank curve recorded at an unmodified PIGE

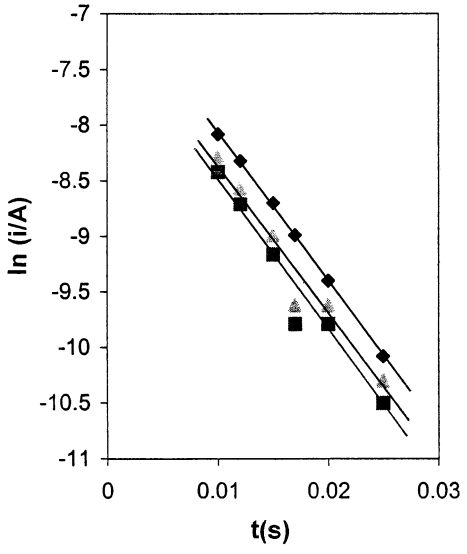

Fig. 7 Plots of ln i versus t (times between 10 ms and 20 ms) for the CA oxidation of different deposits of indigo attached to PIGE. Data from the working curve obtained by subtracting the blank curve recorded at an unmodified PIGE. Applied potential: +550 mV. Electrolyte: aqueous acetate buffer (total concentration 0.50 M) at pH 5.04

ranging between 4×10^{-8} cm and 4×10^{-9} cm). Comparable results are obtained for χ_{min} (model c, restricted electron diffusion).

Proton and electron diffusion

The low charge values experimentally determined suggest that the models b (restricted proton diffusion) and c (restricted electron diffusion), rather than the model a (unrestricted diffusion), may apply. This is in agreement with the linear dependency of ln i on t obtained from long time CAs. If the model b applies, the coefficient of diffusion of protons and the thickness of the electroactive layer can easily be calculated from the ordinate at the origin, OO, and the slope, SL, of such representations using Eq. 11 as $D_H = e^{(OO)}/3.3nFNca$ and $\delta = (2\pi^2 D_H/4(SL))^{1/2}$. If the model c is operative, a similar linear dependency of ln i on t must be obtained. Here, the coefficient of diffusion of electrons and the thickness of the electroactive layer can be calculated using Eq. 12 from the slope and the ordinate at the origin of such representations as $\chi = (e^{(OO)}/(SL))(\pi^2/8nNFa^2c)$ and $D_e = (e^{2(OO)}/(SL))(\pi^2/16n^2 N^2 F^2 a^4 c^2)$.

Assuming, as previously discussed, that the dye deposits (typically 1.5 mg, density 1.35 g cm^{-3}) are composed by a set of cuboid microcrystals of 5 μm size, and using the experimentally determined values of the slope, SL, and the y-intercept, OO, of ln i versus t plots, one obtain consistent values of D_H and δ for the b model. Thus, using Eq. 11, D_H values appear to vary with the pH and are close to 5×10^{-10} cm^2 s^{-1} while δ values approach to 2×10^{-6} cm. In contrast, inconsistent values of such parameters are obtained for the model c using Eq. 12. Here, using the SL and OO values derived from experimental data and the aforementioned parameters, one obtain D_e values close to 6×10^{-15} cm^2 s^{-1}, a value considerably lower than those determined for redox polymers and zeolite-associated metal complexes (between 10^{-8} cm^2 s^{-1} and 10^{-11} cm^2 s^{-1}, vide infra), where one can expect a more uneasy electron hopping. Accordingly, one can conclude that, under our experimental conditions, a model assuming restricted proton diffusion is operative.

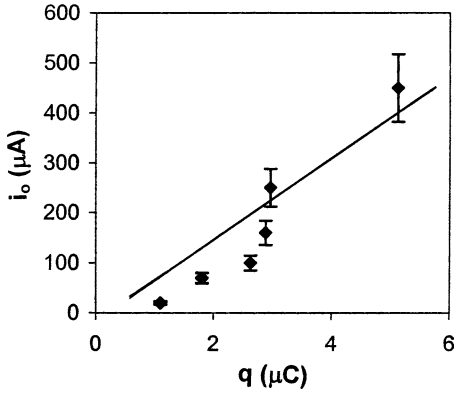

Fig. 8 Plots of q versus i_o for the oxidation of different indigo deposits at pH 5.57. From CAs performed at a potential of +600 mV after subtracting blank CAs at bare PIGE electrodes

Table 1 Number of cuboids, total charge passed during chronoamperometric experiments and minimum thickness of the electroactive layer for indigo-modified PIGEs immersed into aqueous electrolytes

pH	Applied potential (mV)	q (C)	δ_{min} (cm)	pH	Applied potential (mV)	q (C)	δ_{min} (cm)
6.85	+475	1.5×10^{-6}	1.7×10^{-9}	6.85	−550	1.0×10^{-6}	1.2×10^{-9}
5.57	+500	3.0×10^{-6}	3.3×10^{-9}	5.57	−500	1.1×10^{-6}	2.3×10^{-9}
5.04	+550	4.8×10^{-6}	5.4×10^{-9}	5.04	−475	2.1×10^{-6}	3.3×10^{-9}
4.17	+600	8.2×10^{-6}	9.2×10^{-9}	4.17	−400	5.1×10^{-6}	8.0×10^{-9}

Mean value from three independent CAs at indigo-modified electrodes containing 0.00015 ± 0.00002 g of the solid. Values of δ_{min} calculated by assuming a uniform distribution of cuboids

Table 2 Values of the coefficients of diffusion of protons and electrons and effective breadth of the electroactive zone of the crystals in the (a) reduction o, and (b) oxidation, of indigo microparticles attached to PIGEs in contact with aqueous electrolytes

pH	D_H ($cm^2\ s^{-1}$)	δ (cm)	C ($A\ s^{1/2}$)	D_e ($cm^2\ s^{-1}$)
Reduction				
6.85	1.2×10^{-10}	2.1×10^{-6}	7.2×10^{-4}	1.5×10^{-6}
6.01	1.2×10^{-10}	2.1×10^{-6}	8.5×10^{-4}	2.0×10^{-6}
5.57	1.3×10^{-10}	2.2×10^{-6}	1.0×10^{-3}	2.6×10^{-6}
5.04	2.4×10^{-10}	2.9×10^{-6}	1.8×10^{-3}	2.1×10^{-6}
4.74	2.7×10^{-10}	3.2×10^{-6}	2.2×10^{-3}	2.7×10^{-6}
4.17	3.7×10^{-10}	3.7×10^{-6}	2.4×10^{-3}	1.7×10^{-6}
Oxidation				
6.85	7.2×10^{-10}	5.1×10^{-6}	8.5×10^{-4}	5.5×10^{-8}
6.01	4.0×10^{-10}	3.7×10^{-6}	6.8×10^{-4}	1.2×10^{-7}
5.57	3.9×10^{-10}	3.6×10^{-6}	1.1×10^{-3}	3.4×10^{-7}
5.04	3.9×10^{-10}	3.6×10^{-6}	1.1×10^{-3}	3.1×10^{-7}
4.74	3.1×10^{-10}	3.2×10^{-6}	1.0×10^{-3}	4.2×10^{-7}
4.17	2.8×10^{-10}	3.1×10^{-6}	1.2×10^{-3}	7.8×10^{-7}

From CAs recorded under conditions of diffusive control after subtracting blank CAs performed at unmodified PIGEs. D_H and δ calculated, as described in text, from Eq. 11 taking $N_c=8.89\times10^5$, $v_m=194\ cm^3\ mol^{-1}$. D_e was calculated from the slope of $it^{1/2}$ versus t plots using Eq. 10

Table 3 Values of the coefficients of diffusion of protons and electrons and effective breadth of the electroactive zone of the crystals in the (a) reduction o, and (b) oxidation, of alizarin, purpurin, luteolin and morin attached to PIGEs in contact with acetate buffer, at pH values of 4.65 and 5.45

Electrode modifier	Applied potential (mV)	pH	D_H ($cm^2\ s^{-1}$)	δ (cm)	D_e ($cm^2\ s^{-1}$)
Reduction					
Alizarin	−650	5.45	2.2×10^{-10}	3.1×10^{-6}	5.4×10^{-7}
Alizarin	−625	4.65	2.3×10^{-10}	3.8×10^{-6}	6.8×10^{-7}
Purpurin	−700	5.45	1.8×10^{-10}	2.8×10^{-6}	4.4×10^{-7}
Purpurin	−675	4.65	2.0×10^{-10}	3.1×10^{-6}	6.6×10^{-7}
Oxidation					
Alizarin	+650	5.45	4.0×10^{-10}	6.2×10^{-6}	2.1×10^{-7}
Alizarin	+675	4.65	2.6×10^{-10}	5.0×10^{-6}	4.1×10^{-7}
Purpurin	+675	5.45	3.8×10^{-10}	7.2×10^{-6}	2.5×10^{-7}
Purpurin	+700	4.65	3.0×10^{-10}	6.8×10^{-6}	3.3×10^{-7}
Luteolin	+500	5.45	1.9×10^{-10}	2.1×10^{-6}	2.4×10^{-7}
Luteolin	+525	4.65	1.3×10^{-10}	2.4×10^{-6}	3.0×10^{-7}
Morin	+475	5.45	1.7×10^{-10}	3.9×10^{-6}	2.0×10^{-7}
Morin	+500	4.65	1.5×10^{-10}	4.1×10^{-6}	3.8×10^{-7}

From CAs recorded under conditions of diffusive control after subtracting blank CAs performed at unmodified PIGEs. D_H and δ calculated, as described in text, from Eq. 11 taking $N_c=8.89\times105$, $v_m=194\ cm^3\ mol^{-1}$. D_e was calculated from the slope of $it^{1/2}$ versus t plots using Eq. 10

The obtained values of D_H and δ values for indigo are summarised in Table 2 for selected pH values. The values estimated for alizarin, purpurin, luteolin and morin at pH 4.65 and 5.45 are shown in Table 3. The calculated effective breadth layer is close to 2×10^{-6} cm in all cases. This value is considerably larger than the minimum thickness value calculated from the charge passed in voltammetric experiments.

The values of D_H are lower than the values of the diffusion coefficient of K^+ into copper(II) hexacyanoferrate(II) reported by Kahlert et al. ($1.49\times10^{-9}\ cm^2\ s^{-1}$) [34] and those calculated for Li^+ and Et_4N^+ cations diffusing in zeolites ($1\times10^{-9}\ cm^2\ s^{-1}$) [35], but larger than those calculated for ferricinium ions in plasma-polymerised vinylferrocene ($5\times10^{-13}\ cm^2\ s^{-1}$) [36].

The values of D_e were calculated from the slope of the $it^{1/2}$ versus t plots (typically $1\times10^{-3}\ A\ s^{-3/2}$) such as in Fig. 6, using the previously calculated values of D_H, as $D_e=v_m^2\ (SL)^2/16n^2F^2N_c^2D_H^2$. The corresponding values for indigo at different pH values are shown in Table 2, whereas, those estimated for alizarin, purpurin, luteolin and morin at pH 4.65 and 5.45 are summarised in Table 3. The calculated values were relatively high and similar for all the studied dyes: close to $7\times10^{-7}\ cm^2\ s^{-1}$ for the oxidation process and $2\times10^{-6}\ cm^2\ s^{-1}$ for the reduction one. Those values are close to typical values for ion diffusion in solution, thus suggesting that a facile electron hopping occurs, in agreement with the highly reversible character of both the oxidation and reduction processes. No systematic variations of D_e on the pH were detected.

D_e values calculated here are larger than those typically reported for redox polymers, typically between $2\times10^{-8}\ cm^2\ s^{-1}$ [20] and $2\times10^{-9}\ cm^2\ s^{-1}$ [36], and electroactive transition metal complexes encapsulated into zeolites ($2\times10^{-11}\ cm^2\ s^{-1}$) [35], but are lower than those reported for copper(II) hexacyanoferrate(II) ($0.10\ cm^2\ s^{-1}$) [34].

Final considerations

Voltammetry and chronoamperometry of microparticles of indigo, alizarin, purpurin, luteolin and morin at-

tached to graphite electrodes in contact with aqueous electrolytes are in close agreement with the predictions from the Lovric–Scholz model for both the reduction and oxidation processes.

The redox process is rapidly exhausted, denoting that the protonation/deprotonation of dye molecules is limited to a shallow layer in the vicinity of the particle/electrolite interface. The maximum thickness of that layer can be estimated as long as 0.6% of the particle breadth. The values of the coefficient of diffusion of protons and electrons in the indigo particles can be calculated from CA data. Diffusion coefficients of protons are dependent on the pH of the electrolyte, with values ranging between 1×10^{-10} cm^2 s^{-1} and 7×10^{-10} cm^2 s^{-1}. The diffusion coefficient of electrons was almost identical for both the oxidation and reduction processes and essentially pH-independent with a typical value of 1×10^{-6} cm^2 s^{-1}.

These results act in support of the validity of the Lovric–Scholz model for describing the voltammetry of solid particles involving proton/electron diffusion in of organic compounds.

Acknowledgements Financial support the I+D+I GV04B/197 Generalitat Valenciana Project is gratefully acknowledged.

References

1. Scholz F, Lange B (1992) Trends Anal Chem 11:359
2. Scholz F, Meyer B (1994) Chem Soc Rev 23:341
3. Scholz F, Meyer B (1989) Electroanalytical chemistry. In: Bard AJ, Rubinstein I (eds) A series of advances, vol 20. Marcel Dekker, New York, pp 1–87
4. Grygar T, Marken F, Schröder U, Scholz F (2002) Collect Czech Chem Commun 67:163
5. Scholz F, Nitschke L, Henrion G (1989) Fresenius Z Anal Chem 334:56
6. Jaworski A, Stojek Z, Scholz F (1993) J Electroanal Chem 354:1
7. Komorsky-Lovric S, Mircevski V, Scholz F (1999) Mikrochim Acta 132:67
8. Bond AM, Marken F, Hill E, Compton RG, Hügel H (1997) J Chem Soc Perkin Trans 2:1735
9. Doménech A, Doménech MT, Saurí MC, Gimeno JV, Bosch F (2003) Anal Bioanal Chem 375:1161
10. Grygar T, Kucková S, Hradil D, Hradilová D (2003) J Solid State Electrochem 7:706
11. Doménech AM, Doménech MT, Saurí, MC (2005) Talanta (in press)
12. Lovric M, Scholz F (1997) J Solid State Electrochem 1:108
13. Lovric M, Scholz F (1999) J Solid State Electrochem 3:172
14. Oldham KB (1998) J Solid State Electrochem 2:367
15. Schröder U, Oldham KB, Myland JC, Mahon PJ, Scholz F (2000) J Solid State Electrochem 4:314
16. Rolison DR, Bessel CA (2000) Acc Chem Res 33:737
17. Downard AJ, Bond AM, Hanton LR, Heath GA (1995) Inorg Chem 34:6387
18. Bond AM, Colton R, Mahon PJ, Tan WT (1997) J Solid State Electrochem 1:53
19. Bond AM, Marken F, Williams ChT, Beattie DA, Keyes TE, Foster RJ, Vos JG (2000) J Phys Chem 104:1977
20. Andrieux CP, Savéant J-M (1988) J Phys Chem 92:6761
21. Wu X-Z, Kitamori T, Sawada T (1992) J Phys Chem 96:9406
22. Lovric M, Hermes M, Scholz F (1998) J Solid State Electrochem 2:401
23. Fernández-Sánchez C, Costa-García A (2000) Electrochem Commun 2:776
24. Komorsky-Lovric S (2000) J Electroanal Chem 482:222
25. Roessler A, Crettenand D, Dossenblach O, Marte W, Rys P (2002) Electrochim Acta 47:1989
26. Roessler A, Crettenand D, Dossenblach O, Marte W, Rys P (2002) J Appl Electrochem 32:647
27. Steenken S, Neta P (1982) J Phys Chem 86:3661
28. Hodnick WF, Milosavljevic EB, Nelson JH, Pardini RS (1988) Biochem Pharmacol 37:2607
29. Amatore C, Lefrou C, Pflüger F (1989) J Electroanal Chem 270:43
30. Garreau D, Hapiot P, Savéant JM (1990) J Electroanal Chem 289:73
31. Evans DH (1990) Chem Rev 90:739
32. Hendrickson HP, Kaufman AD, Lunte GE (1994) J Pharm Biomed Anal 12:325
33. Petit Chr Nagy A, Quarin G, Kauffmann JM (1996) J Pharm Belg 51:1
34. Kahlert H, Retter U, Lohse H, Siegler K, Scholz F (1998) J Phys Chem 102:8757
35. Doménech A (2004) J Phys Chem 108:20471
36. Daumm P, Lenhard JR, Rolison D, Murray RW (1980) J Am Chem Soc 102:4649